LETTERS

Vitrification of a monatomic metallic liquid

M. H. Bhat[1], V. Molinero[1,2], E. Soignard[1], V. C. Solomon[1], S. Sastry[3], J. L. Yarger[1] & C. A. Angell[1]

Although the majority of glasses in use in technology are complex mixtures of oxides or chalcogenides, there are numerous examples of pure substances—'glassformers'—that also fail to crystallize during cooling. Most glassformers are organic molecular systems, but there are important inorganic examples too[1,2], such as silicon dioxide and elemental selenium (the latter being polymeric). Bulk metallic glasses can now be made[3]; but, with the exception of $Zr_{50}Cu_{50}$ (ref. 4), they require multiple components to avoid crystallization during normal liquid cooling. Two-component 'met-glasses' can often be achieved by hyperquenching, but this has not hitherto been achieved with a single-component system. Glasses form when crystal nucleation rates are slow, although the factors that create the slow nucleation conditions are not well understood. Here we apply the insights gained in a recent molecular dynamics simulation study[5] to create conditions for successful vitrification of metallic liquid germanium. Our results also provide micrographic evidence for a rare polyamorphic transition preceding crystallization of the diamond cubic phase.

It has been argued that any liquid can be vitrified if the cooling rate is sufficiently high[6], and even ideal gases can be vitrified if the molecules are allowed complex shapes[7]. It seems that the crystal nucleation time can be made long with respect to amorphous form assembly times in a variety of ways, for instance by making sure that not more than a few atoms are hot at any time. Thus amorphous forms of metals like Bi and Pb have been made by deposition from the vapour at very low temperatures[8]. However, these prove to have no kinetic stability, and crystallize when the temperature is raised even 15 K above absolute zero. In spite of the conclusions of ref. 6, vitrification of single-component metals by cooling from the liquid might therefore seem improbable.

On the other hand, we demonstrated recently[5] by molecular dynamics that an atomic liquid, Stillinger–Weber silicon, becomes non-crystallizing in 'slow' molecular dynamics cooling runs when the interaction potential is modified, without reducing the attractive potential, so as to lower the melting point by ~50% and put isoenergetic crystals in competition with each other against increasingly stabilized liquid. We found that ability to vitrify on the computational timescale was established when the diffusivity of the liquid at the crystallization temperature was reduced to 1.0×10^{-5} cm^2 s^{-1}, and the excess free energy, which provides the drive to crystallize below the melting temperature T_m, rose most slowly during supercooling. These turn out to be the same conditions established[9] in experiments on binary alloys such as Ni-P (ref. 10) and Zr_2Ni, which are vitrifiable by melt spinning. (In these cases, the melting point of Ni is lowered by 35%, and Zr by 42%, as a result of chemical mixing in which an optimum negative deviation from ideal mixing is exploited[3,6]. In Zr-Cu, a 'bulk' glassformer at 1:1, a metastable eutectic[4] lies lower still).

These results suggested to us that another variable, pressure, might be used to achieve the same conditions for a single-component metal of the right initial properties. Pressure can only lower the melting point if the melting is accompanied by a volume decrease, so the possibilities, starting at zero pressure, are limited to Bi, Ga, Ce, Si and Ge. Having used liquid Si as the starting point in our 'potential tuning' study[5], it was natural to choose liquid Si for initial tests of the new proposal, using molecular dynamics simulation of the Stillinger–Weber silicon potential[11].

At the solid–solid–liquid triple point T_3 of Si, $T_3/T_m(1$ atm$)$ is 0.5 (see Methods and Supplementary Information), and simulations with the Stillinger–Weber potential have found[12] (see Methods and Supplementary Information) that its diffusivity at T_3 was 0.9×10^{-5} cm^2 s^{-1}, as in the Ni-P eutectic. Encouraged by these relations and also by Brazhkin's observations on In-Sb (ref. 13), and Tanaka's arguments[14], but having failed to vitrify Si with multianvil cell quenching at 9 GPa (see Supplementary Information), we turned our attention to experiments conducted in a high-pressure diamond anvil cell (DAC).

In DACs, the transparency of the compressing diamonds permits the use of pulsed-laser-beam melting methods. The high thermal conductivity of the diamonds ensures rapid cooling of the samples. The optimum melting conditions were determined by variation of laser pulse duration, sample size, and thickness of the pressure-transmitting (NaCl) medium.

As sample for the diamond cell study, we chose Ge for several reasons. First, we thought Ge, which has a larger effective hard core than Si but the same sp^3-based tetrahedral bonding, might be closer in character to the model monatomic glassformer of our earlier (zero-pressure) study[5], as indeed we verify below. Second, Ge, in the normal-pressure (1 atm) liquid state, has a higher first-shell coordination number than liquid Si, and is considered to resemble a disordered β-tin structure[15]. It has a metallic value and temperature coefficient of electrical conductivity[16], and should behave more obviously like a metal under high-pressure conditions where the electron delocalization must be higher still. Third, partial vitrification of Ge in belt-type anvil press quenches has been reported[17]. Finally, Ge has little affinity for carbon, and hence is less likely to chemically damage the DAC windows during melting experiments. Subsequently, the molecular dynamics of liquid Ge (discussed later) yields a diffusivity of only 0.76×10^{-5} cm^2 s^{-1} at T_3, even lower than for Si.

Using the sample mountings described in the Methods section, we prepared 20-μm-diameter Ge samples, melt-quenched from pressures in the range 5–11 GPa (the upper limit for our diamond culets), for *in situ* Raman, and *ex situ* transmission electron microscope (TEM) examination. The Raman spectra for pressures above 7.9 GPa (by ruby fluorescence) showed the disappearance of the sharp intense line at 326 cm^{-1} (298 cm^{-1} at 0 GPa) and its replacement by a featureless broad fluorescence band, from which no structural details could be obtained.

The pressures, after the quench, were found to differ from the initial value by ±0.8 GPa, so we report results as the initial pressure with the final pressure in parentheses. In repeat experiments, glasses are always obtained at 7.9 GPa and above, ~11 GPa being our

[1]Department of Chemistry and Biochemistry, Arizona State University, Tempe, Arizona 85287-1604, USA. [2]Department of Chemistry, University of Utah, Salt Lake City, Utah 84112-0850, USA. [3]J. Nehru Centre for Advanced Scientific Research, Jakkur Campus, Bangalore 560064, India.

maximum. Four trials at ~5 GPa (including one using green laser heating) failed to vitrify. Attempts to characterize a vitreous sample *in situ* (under pressure) by X-ray diffraction using the Sector 1 Advanced Photon Source (APS) at Argonne, unfortunately were not successful owing to the very small sample size. The TEM results, by contrast, provided detailed evidence that vitreous Ge was produced directly from the melt in the case of quenches of small samples at pressures near T_3.

Figure 1a and b shows twin optical microscope images of the DAC aperture with embedded Ge crystals before, and spread glass after, the melting pulse. The TEM image in Fig. 1c shows a ~300-nm-tall
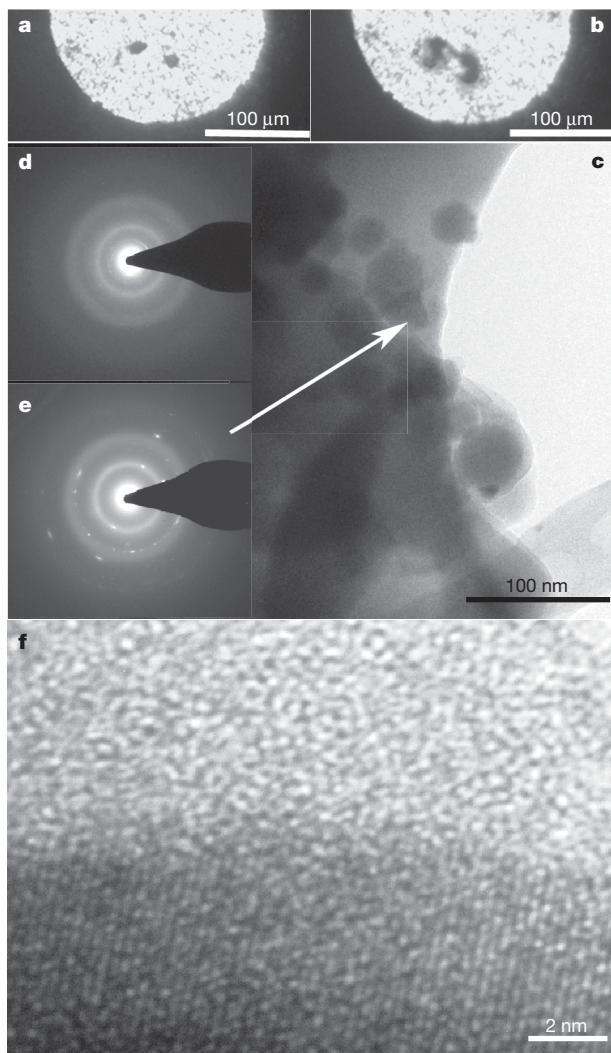
Figure 1 | Optical and electron micrographs of vitrified Ge. a, b, The Ge sample through the gasket aperture (between the diamond anvils) before and after the melting pulse. **c,** 300 nm segment of the 2 μm sample fragment of vitrified Ge quenched at 7.9(7.1) GPa, showing globules in matrix. Energy-dispersive X-ray analysis of both shows only Ge and Cu (from the grid) to be present. **d,** Amorphous diffraction pattern obtained from all areas except the area including the globule indicated by the arrowhead. **e,** Amorphous diffraction pattern for the globule area. Laue spots, indicating crystalline character, are obvious. The crystal–glass boundary (at the arrow tip) is seen in the high-resolution image of **f**. The crystal has grown within a globule. Energy-dispersive X-ray analysis of both shows only Ge and Cu (from the grid) present (see Supplementary Information). Other globules in **c** are fully amorphous. This is reminiscent of the preferential crystallization of the LDA in Al_2O_3–Y_2O_3 polyamorphic transitions[29], and also in the molecular triphenyl phosphite case[30]. Annular dark-field imaging (see Supplementary Information) proves that the globules in **c** are darker because they are thicker, protruding from the matrix as seen at the right edge of **c**. In the annular dark field they appear bright.

section of a 2 μm sample from a quench at 7.9(7.1) GPa, with two adjacent electron diffractograms (Fig. 1d and e). Figure 1d is from one of several electron-thin regions that gave the same diffraction pattern. Also, in subsequent studies of samples melt-quenched in the favourable pressure range, the same pattern is obtained. It is clearly an 'amorphous' pattern, being devoid of any irregularities or inhomogeneities that could be attributed to nanocrystals. Figure 1e is taken from a small area that includes a globule of interest to our discussion (at arrowhead), and contains a number of spots in addition to the diffuse rings. The spots are due to a single diamond-cubic Ge crystal originating within the globule (see high-resolution image in Fig. 1f). Globules with and without similar embedded crystals were seen in other sections of the 2 μm fragment (Fig. 1c, which is a small part of the sample in Fig. 1b). The TEM image (Fig. 1c) was chosen over those from other successful runs (all of which gave the same amorphous diffractograms), because of the presence of the globular features—see our discussion below. The globular sample, the importance of which we discuss below, was obtained at the low-pressure limit (7.9(7.1) GPa) of the range for successful vitrifications. All other vitrified samples had uniform textures. The structure factor for the glassy phase has been derived from the diffractogram and is compared with other relevant data in Fig. 2.

Thus far we have tested the vitrifiability of liquid Ge near its triple point. Clearly metallic, even at normal pressure, liquid Ge yields vitreous states when melt-quenched in the DAC from near and somewhat above the triple point pressure, but not from much below it. The possibility that the quench product is a β-tin-like (or other high-density) crystal, which then amorphizes during decompression is eliminated by our temperature of decompression, 25 °C, because much work has shown that ambient decompression of metastable metal crystals of this type, including Ge[18], yields crystalline semiconductors. Details on five such possible paths for Ge, all documented, all with the same conclusion, are given in Supplementary
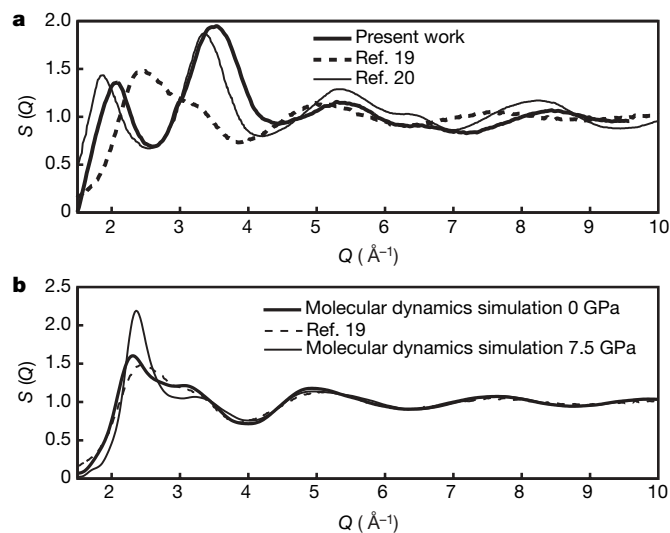
Figure 2 | Comparisons of structure factors for vitreous and liquid states of Ge from laboratory and molecular dynamics simulation studies. a, Structure factor $S(Q)$ (that is, the scattered intensity at the scattering vector Q) for glassy Ge derived from the electron diffraction pattern of Fig. 1 (thick solid line) compared with the corresponding TEM electron-diffraction-based $S(Q)$ for vapour-deposited amorphous Ge[20] (thin solid line). The thick dashed line is $S(Q)$ at 1,273 K from liquid Ge[19]. The similarity of the present $S(Q)$ to that of the vapour-deposited value confirms the LDA character, while the displacement of the peaks to higher Q for our sample reflect its formation at pressure exceeding zero. **b,** Our Ge simulation results for the liquid at zero pressure (thick solid line), and at 7.5 GPa (thin solid line) showing agreement with laboratory results[19] at zero pressure and 1,273 K (dashed line). Small Q changes reflect mainly changes in second-, third- and higher-shell coordination numbers.

Information. We conclude that our successful quenches have yielded the first examples of vitrification of a monatomic metallic liquid.

However, just as the high-pressure crystals are known not to survive decompression to ambient pressure unless first cooled below 100 K, so also a metallic glass does not survive our ambient-temperature decompression. Rather, it transforms from a high-density amorphous (HDA) glass to a low-density amorphous (LDA) glass. We now verify that we have observed the LDA (in Fig. 1). To aid our analysis we use additional simulations on a model of Ge (V.M., manuscript in preparation) similar to one used to study Ge surfaces (see Supplementary Information) for which no comparisons with experiments were made. We make comparisons in Fig. 2.

Figure 2b shows the excellent agreement of calculated and observed[19] structure factors of liquid Ge at normal pressure, and also the effect of pressure increase to 7.5 GPa. The latter effect is confirmed by *ab initio* molecular dynamics studies[15] analysed in terms of increasing metallicity. A glass formed from this liquid should be unambiguously metallic. However, the Fig. 2a structure factor for our glass, derived from the Fig. 1d diffraction pattern, is strikingly different from that of the liquid[19]. As anticipated above, it closely resembles that obtained from electron diffraction of vapour-deposited Ge[20] (the LDA non-metallic form), and also from X-ray scattering for vapour-deposited[21] and electrodeposited Ge (see Supplementary Information). The differences between the high- and low-density forms are shared by water, Si and Ge[22].

The identification of our glass with the previous LDAs seems unambiguous. Our finding is consistent with that of ref. 13 in the only parallel of our work—the high-pressure vitrification of liquid GaSb. (GaSb at 1 atm is a zincblende phase with a low melting point of 970 K, decreasing with increasing pressure to 670 K at T_3). Again, the dense polyamorph does not survive decompression at room temperature. Indeed, this is expected from the theoretical model[23] which first predicted the liquid–liquid transitions: Aptekar[23] showed a spinodal limit on the stability of both HDA Ge and Si at 2–4 GPa (see also Supplementary Information).

To identify the liquid–liquid transition, we turn to a composite phase diagram (Fig. 3) that combines what we know from the earlier simulation study[5] with what we know from laboratory high-pressure[24] and supercooling studies[25]. Figure 3 shows a temperature–pressure phase diagram for Ge, whose vertical axis is projected from the temperature–λ phase diagram[5] at $\lambda = 20$ (versus $\lambda = 21$ for Si), as shown to be appropriate by the $(S(Q))$ comparisons in Fig. 2b. (λ is the 'tetrahedrality parameter' in the Stillinger–Weber potential[5,11].) We emphasize the projection of the liquid–liquid transition line of the temperature–λ phase diagram into the pressure plane of the temperature–pressure phase diagram.

Pressure increases depress not only the melting point of Ge, but also the liquid–liquid transition[26], as predicted in refs 23 and 27 and as observed by molecular dynamics for Stillinger–Weber Si (ref. 12; V.M., S.S. and C.A.A.,unpublished work). We represent the glass transition temperature T_g by a thick square-dotted line, using the observation[12] (for Stillinger–Weber Si) that isothermal diffusivity passes though a maximum below the T_3 pressure and that T_g must be above 473 K at 8.1(8.9) GPa, because heating an *in situ* vitrified sample up to 473 K (the pressurized cell safety limit) for one hour did not cause crystallization (according to Raman spectra). We represent the quenches of this study on the phase diagram of Fig. 3 (see lines a, b and c).

The lower-pressure, crystallizing, melt-quenches of our current experiments are represented by the vertical dashed line 'a' that passes through the liquid–liquid line while the liquid is still well above the extension of the T_g line. Crystals form rapidly as they cross the liquid–liquid line[5,12,26] because the gap in configuration space between LDA and crystal is so much smaller than that between HDA and the crystal[5].

The melt-quenches that produce amorphous Ge without globules are represented by vertical line 'c'. Above T_3, the liquid–liquid line is almost vertical (see caption and Supplementary Information). Thus, above T_3 there is no possibility that the liquid can transform to LDA before it vitrifies. The homogeneous glass obtained at 10.6(10.1) GPa
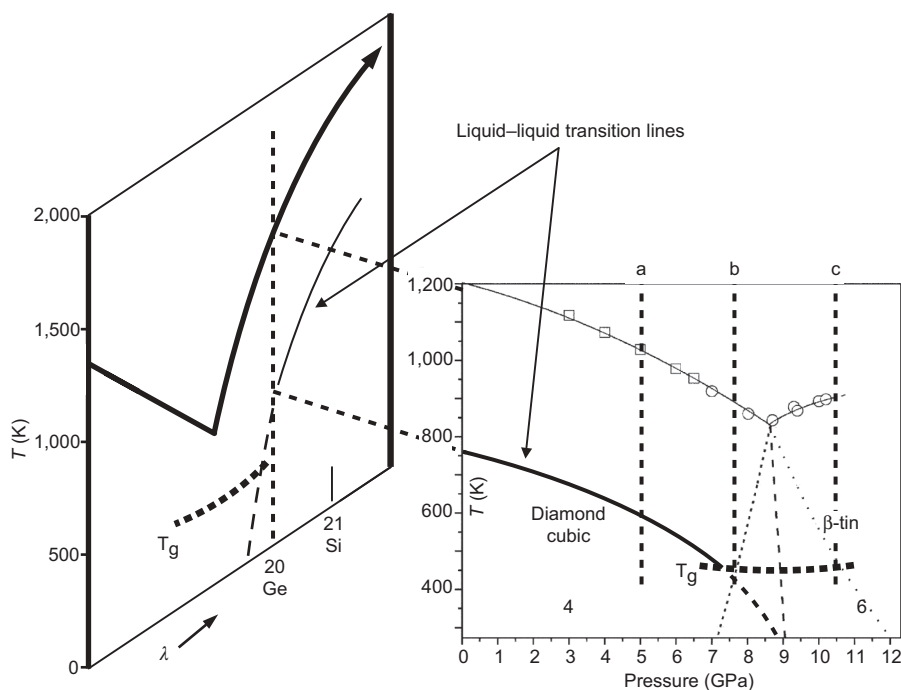
Figure 3 | Relation of temperature–pressure phase diagram for Ge to the temperature–λ potential diagram for Stillinger–Weber systems. The temperature–pressure phase diagram for Ge[24] is shown in relation to the temperature–λ phase diagram of ref. 5 by which the relation of Ge to Si in the temperature–λ diagram is understood. The temperature scale changes for Ge, and becomes that of the laboratory Ge phase diagram, and the gap between T_m and the liquid–liquid transition temperature T_{LL} has been set to the experimental supercooling limit found by cooling small levitated samples[25]. Projections of the temperature–λ diagram at $\lambda = 20$ into the pressure plane show how the T_m and T_{LL} transition lines of Ge change with pressure. The T_{LL} line is shown approaching the vertical at the T_3 pressure, for thermodynamic reasons given in ref. 5. In water polymorphism[32], T_{LL}, which goes vertical at the T_3 pressure, tracks the homogeneous crystal nucleation line T_h. T_h, much studied in solution systems where composition replaces the pressure axis, goes almost vertical near the eutectic composition (the equivalent of the T_3 pressure), intersecting the ideal glass and Kauzmann temperatures T_0 and T_K at the eutectic temperature (see Supplementary Information). Therefore, LDA cannot form during cooling above the T_3 pressure, for example, along line 'c'. For a description of the vertical dashed lines 'a', 'b' and 'c', see text. The numbers '4' and '6' indicate the coordination numbers of crystal phases.

must therefore be the HDA metallic form. Thus we have vitrified a metallic liquid into a metallic glass. As argued above (see details in Supplementary Information), this metallic glass transforms to LDA during ambient decompression, via spinodal collapse[23,28].

The vertical line 'b' is the cooling trajectory of the sample that yielded the globule phase as a consequence of passing the liquid–liquid line and the T_g line almost simultaneously. Then, as seen in Y_2O_3–Al_2O_3 glass[29] and also in triphenyl phosphite[30], nucleated droplets of the LDA phase are vitrified as they form (LDA being less diffusive than HDA). Given the propensity of low-temperature liquid polyamorphs to crystallize[29,30], the existence of nanocrystals within many, but not all, of the amorphous globules then provides circumstantial microscopic evidence for the controversial liquid–liquid transition in Si-like supercooled liquids[12,26,31].

METHODS SUMMARY

DAC studies. Crystalline Ge samples were embedded in a thin layer of pressure-distributing NaCl inside a $210\,\mu m$ hole in a T-301 stainless steel gasket, which was mounted in a Merrill-Bassett DAC. Ruby chips were included for pressure determination using the fluorescence spectrum frequency shift. A Synrad 60-1 CO_2 laser provided 125 W pulses of duration 2–$100\,\mu s$ in trial experiments. Glass formation was initially inferred from the disappearance of the strong Raman signal for diamond-cubic Ge at $326\,cm^{-1}$ (7.9 GPa). The Ge sample (Fig. 1b), embedded in NaCl, was then carefully transferred onto a TEM copper grid (Ted Pella, Inc.) with lacey carbon support, and the NaCl carefully dissolved away using distilled water, which usually leaves the Ge on the grid. The high-resolution images and selected area diffraction patterns were recorded with a Philips CM200 field emission gun electron microscope operated at 200 kV. The instrument is equipped with a Gatan slow-scan charge-coupled device (CCD) camera, an energy-dispersive X-ray detector (EDAX) and the Gatan-Digital Micrograph and ES Vision acquisition systems.

Data treatment. Diffraction data for amorphous Ge were collected on the above-mentioned high-resolution TEM and calibrated using an Au standard. The two-dimensional diffraction image was radially integrated and scaled to the Dirac–Fock atomic form factors (200 keV electrons)[33]. The resulting structure factor $S(Q)$ is shown in Fig. 2.

Molecular dynamics simulations summary. The Stillinger–Weber Si simulations[11] were performed with protocols described in ref. 4. For Ge, periodic isobaric-isothermal simulations of 5,000 atoms modelled with the Stillinger–Weber[11] potential modified with $\lambda = 20$, $\varepsilon = 45\,kcal\,mol^{-1}$ and $\sigma = 2.1836\,Å$ were carried out using the LAMMPS code (see Methods and Supplementary Information).

Full Methods and any associated references are available in the online version of the paper at www.nature.com/nature.

Received 5 February; accepted 21 June 2007.

1. Privalko, Y. Excess entropies and related quantities in glass-forming liquids. *J. Phys. Chem.* **84**, 3307–3312 (1980).
2. Martinez, L. M. & Angell, C. A. A thermodynamic connection to the fragility of glass-forming liquids. *Nature* **410**, 663–667 (2001).
3. Johnson, W. L. Bulk glass-forming metallic alloys: science and technology. *Mater. Res. Soc. Bull.* **24**, 42–50 (1999).
4. Wang, W. H., Lewandowski, J. J. & Greer, A. L. Understanding the glass-forming ability of Cu50Zr50 alloys in terms of a metastable eutectic. *J. Mater. Res.* **20**, 2307–2313 (2005).
5. Molinero, V., Sastry, S. & Angell, C. A. Tuning of tetrahedrality in a silicon potential yields a series of monatomic (metal-like) glasse formers of very high fragility. *Phys. Rev. Lett.* **97**, 075701 (2006).
6. Cohen, M. H. & Turnbull, D. Composition requirements for glass formation in metallic and ionic systems. *Nature* **189**, 131–132 (1961).
7. van Ketel, W., Das, C. & Frenkel, D. Structural arrest in an ideal gas. *Phys. Rev. Lett.* **94**, 135703 (2005).
8. Hilsch, R. in *Non-Crystalline Solids* (ed. Frechette, V. D.) 348 (J. Wiley and Sons, New York, 1960).
9. Chathoth, S. M., Meyer, A., Koza, M. M. & Juranyi, F. Atomic diffusion in liquid Ni, NiP, PdNiP, and PdNiCuP alloys. *Appl. Phys. Lett.* **85**, 4881–4883 (2004).
10. Wachtel, E. *et al.* Magnetic-susceptibility and DSC study of the crystallization of melt-quenched Ni-P amorphous-alloys. *Mater. Sci. Eng. A* **133**, 196–199 (1991).
11. Stillinger, F. H. & Weber, T. A. Computer-simulation of local order in condensed phases of silicon. *Phys. Rev. B* **31**, 5262–5271 (1985).
12. Angell, C. A., Borick, S. & Grabow, M. Glass transitions and first order liquid-metal-to-semiconductor transitions in 4–5–6 covalent systems. *J. Non-Cryst. Solids* **207**, 463–471 (1996).
13. Brazhkin, V. V., Larchev, V. I., Popova, S. V. & Skrotskaya, G. G. The influence of high pressure on the disordering of the crystal structure of solids rapidly quenched from the melt. *Phys. Scr.* **39**, 338–340 (1989).
14. Tanaka, H. Simple view of waterlike anomalies of atomic liquids with directional bonding. *Phys. Rev. B* **66**, 064202 (2002).
15. Koga, J., Nishio, K., Yamaguchi, T. & Yonezawa, F. Tight-binding molecular dynamics study on the structural change of amorphous germanium with the increase of density. *J. Phys. Soc. Jpn* **73**, 388–396 (2004).
16. Schnydersy, H. S. & Van Zytveldz, J. B. Electrical resistivity and thermopower of liquid Ge and Si. *J. Phys. Condens. Matter* **8**, 10875–10883 (1996).
17. Zhang, F. X. & Wang, W. K. Microstructure of germanium quenched from the undercooled melt at high-pressures. *Appl. Phys. Lett.* **67**, 617–619 (1995).
18. Brazhkin, V. V., Lyapin, A. G., Popova, S. V. & Voloshin, R. N. Non-equilibrium phase transitions and amorphization in Si, Si/GaAs, Ge, and Ge/GaSb at the decompression of high-pressure phases. *Phys. Rev. B* **51**, 7549–7554 (1995).
19. Salmon, P. S. A. Neutron-diffraction study on the structure of liquid germanium. *J. Phys. F* **18**, 2345–2352 (1988).
20. Ankele, J., Mayer, J., Lamparter, P. & Steeb, S. Structure factor of amorphous-germanium by quantitative electron-diffraction. *J. Non-Cryst. Solids* **193**, 679–682 (1995).
21. Etherington, G. *et al.* A neutron-diffraction study of the structure of evaporated amorphous-germanium. *J. Non-Cryst. Solids* **48**, 265–289 (1982).
22. Benmore, C. J. *et al.* Intermediate range chemical ordering in amorphous and liquid water, Si, and Ge. *Phys. Rev. B* **72**, 132201(4) (2005).
23. Aptekar, L. I. Phase transitions in non-crystalline germanium and silicon. *Sov. Phys. Dokl.* **24**, 993–995 (1979).
24. Voronin, G. A. *et al.* In situ X-ray diffraction study of germanium at pressures up to 11 GPa and temperatures up to 950 K. *J. Phys. Chem. Solids* **64**, 2113–2119 (2003).
25. Li, D. & Herbach, D. M. Containerless solidification of germanium by electromagnetic levitatioins and in a drop-tube. *J. Mater. Sci.* **32**, 1437–1442 (1997).
26. Sastry, S. & Angell, C. A. Liquid–liquid phase transition in supercooled liquid silicon. *Nature Mater.* **2**, 739–743 (2003).
27. Ponyatovsky, G. G. A thermodynamic approach to T-P phase diagrams of substances in liquid and amorphous states. *J. Phys. Condens. Matter* **15**, 6123–6141 (2003).
28. Mishima, O. Reversible transition between two H_2O amorphs at ~0.2 GPa and ~135 K. *J. Chem. Phys.* **100**, 5910–5919 (1991).
29. Aasland, S. & McMillan, P. F. Density-driven liquid–liquid phase-separation in the system Al_2O_3–Y_2O_3. *Nature* **369**, 633–636 (1994).
30. Kurita, R. & Tanaka, H. Critical-like phenomena associated with liquid-liquid transition in a molecular liquid. *Science* **306**, 845–848 (2004).
31. Spaepen, F. & Turnbull, D. in *Laser-Solid Interactions and Laser Processing 1978* (eds Ferris, S. D., Leamy, H. J. & Poate, J.) *AIP Conf. Proc.* **50**, 73–83 (1979).
32. Stanley, H. E. *et al.* The puzzling behavior of water at very low temperature. *Phys. Chem. Chem. Phys.* **2**, 1551–1558 (2000).
33. Rez, D., Rez, P. & Grant, I. Dirac-Fock calculations of X-ray scattering factors and contributions to the mean inner potential for electron scattering. *Acta Crystallogr. A* **50**, 481–497 (1994).

METHODS

Molecular dynamics simulations on Stillinger–Weber Si and Ge. Molecular Dynamics (MD) simulations of Si with the Stillinger–Weber[11] potential were executed at different pressures from 0 to 16 GPa, and those carried out in the vicinity of the triple point (~11 GPa) and up to 16 GPa never crystallized. Higher pressures were not investigated. The diffusivity at the triple point was $0.96 \times 10^{-5}\,\mathrm{cm}^2\,\mathrm{s}^{-1}$.

The simulations presented in the letter were carried on a model of Ge based on the Stillinger–Weber potential for Si with tetrahedrality parameter $\lambda = 20$, and scaling the two-body attraction term to reproduce the crystal energy of Ge, $\varepsilon = 45\,\mathrm{kcal\,mol}^{-1}$ and $\sigma = 2.1836\,\text{Å}$ (V.M., manuscript in preparation). These runs were executed using a fast parallel-processing MD code (LAMMPS code[34]), and periodic boundary conditions, with isobaric–isothermal simulations on 5,000 atoms. A similar model with $\lambda = 19.5$ has been used to study solid Ge surfaces[35], and was recently applied to liquid Ge-Si alloys[36].

As seen in Fig. 2b, the agreement of the Ge simulations with experiment is very good, minor differences only showing up at small Q, where the second and third and higher neighbour shells are involved. According to this model, the diffusivity at the triple point, $0.76 \times 10^{-5}\,\mathrm{cm}^2\,\mathrm{s}^{-1}$, is even lower than it is for Si, implying that crystallization would never be observed on any computational timescale.

34. Plimpton, S. Fast parallel algorithms for short-range molecular-dynamics. *J. Comput. Phys.* **117**, 1–19 (1995).
35. Grabow, M. H. & Gilmer, G. H. Thin-film growth modes, wetting and cluster nucleation. *Surf. Sci.* **194**, 333–346 (1988).
36. Yu, W. B. & Stroud, D. Molecular-dynamics study of surface segregation in liquid semiconductor alloys. *Phys. Rev. B* **56**, 12243–12249 (1997).